

# Geometric phase for twisted photons

Li-Ping Yang<sup>1,\*</sup>

<sup>1</sup>Center for Quantum Sciences and School of Physics, Northeast Normal University, Changchun 130024, China

We use a purely geometric method to understand the rotation of the photonic polarization vector in an optical fiber without birefringence. This rotation was explained due to Berry's phase of spin-1 photons. Via our method, we predict similar geometric rotations also exist for twisted photons carrying orbital angular momentum (OAM). The corresponding geometric phase can be applied in photonic OAM-state-based quantum computation and quantum sensing.

In the 1980s, the geometric rotation of the polarization vector of light was observed in a helically wound single-mode fiber by Ross [1] and other researchers [2]. This phenomenon was later explained due to the Berry's phase [3]  $\gamma(C) = -2\pi m_s(1 - \cos \theta)$  of spin-1 ( $m_s = 1$ ) photons travelling on a helix with pitch angle  $\theta$  by Chiao and Wu [4]. Tomita and Chiao experimentally verified this photonic Berry's phase of more general fiber configurations with non-uniform torsion [5]. In Chiao and Wu's quantum description [4], the helicity of photons  $\hat{S} \cdot \mathbf{k}/|\mathbf{k}|$ , which is the projection of photon spin on the wave vector  $\mathbf{k}$  axis, is an adiabatic invariant during propagation. Thus, the photon spin states could accumulate Berry's phase when moving in the parameter (reciprocal) space  $(k_x, k_y, k_z)$ . Berry constructed a Schrödinger-like equation with an effective photon-spin Hamiltonian for electromagnetic field propagating in a mono-mode fiber to complete this quantum interpretation [6]. In addition to the photon helicity, the projection of the photonic OAM  $\langle \hat{\mathbf{L}} \cdot \mathbf{e}_z \rangle$  on the propagating direction  $\mathbf{e}_z$  is also conserved [7, 8]. An interesting question arises does a similar geometric rotation exist for the OAM degrees of freedom of photons? In this work, we show the answer is yes.

In parallel to the quantum Berry-phase-based description [4, 6], classical geometric interpretations of the anholonomy of coiled light have also been proposed [1, 9, 10]. Inspired by these insights, we give a different explanation for this rotation by combining differential geometry of the coiled fiber path and reflections of photons in the fiber. The key idea is to evaluate the rotation of the photon coordinate frame (PCF) with respect to the local coordinate frame (LCF) parallelly transporting on the fiber. We prove that the LCF always recovers its initial configuration after one circulation if the two ends of the fiber are parallel. Then, the rotation of the PCF leads to the rotation of the polarization of the light, i.e., the previous geometric phase of photon spin states [4]. Applying our theory on a twisted photon, we predict that a photon carrying OAM  $m\hbar$  will acquire a geometric phase  $\gamma_m(C) = 2m\pi \cos \theta$  after one helical circulation.

*Parallel transport of the local coordinate frame*—The unit tangent vector  $\mathbf{t}(s)$ , normal vector  $\mathbf{n}(s)$ , and binormal vector  $\mathbf{b}(s)$  form a LCF on the fiber at  $s$  as shown in Fig. 1 (a). When a curve is parametrized by the arc length, the dynamics of the

LCF is governed by Frenet formulas [11]

$$\frac{d}{ds} \mathbf{n}(s) = -\kappa(s) \mathbf{t}(s) - \tau(s) \mathbf{b}(s), \quad (1)$$

$$\frac{d}{ds} \mathbf{b}(s) = \tau(s) \mathbf{n}(s), \quad (2)$$

$$\frac{d}{ds} \mathbf{t}(s) = \kappa(s) \mathbf{n}(s), \quad (3)$$

where  $\kappa(s)$  and  $\tau(s)$  are the curvature and torsion of the curve at  $s$ , respectively.

For a uniform helix, its curvature  $\kappa$  and torsion  $\tau$  are constants. The dynamic evolution of the LCF is given by,

$$\hat{R}(\varphi, \mathbf{e}) =$$

$$\begin{bmatrix} \cos \varphi & -\cos \theta \sin \varphi & -\sin \theta \sin \varphi \\ \cos \theta \sin \varphi & \sin^2 \theta + \cos^2 \theta \cos \varphi & -\sin \theta \cos \theta (1 - \cos \varphi) \\ \sin \theta \sin \varphi & -\sin \theta \cos \theta (1 - \cos \varphi) & \sin^2 \theta \cos \varphi + \cos^2 \theta \end{bmatrix}, \quad (4)$$

which is the rotation around the axis  $\mathbf{e} = [0, -\sin \theta, \cos \theta]$  with  $\sin \theta = \kappa/\omega$ ,  $\cos \theta = \tau/\omega$ , and  $\omega = \sqrt{\kappa^2 + \tau^2}$ . Here  $\varphi = \omega s$  is the azimuth angle. We can verify that  $\hat{R}(2\pi, \mathbf{e})$  equals to the identity matrix  $\hat{I}$ . Thus, the LCF returns its initial configuration in the stationary laboratory reference frame. Next, we will show that this result is still valid for a non-uniform helix if two ends of the curve are parallel.

Considering an arbitrary vector  $\mathbf{v} = v_n \mathbf{n} + v_b \mathbf{b} + v_t \mathbf{t}$  co-moving with the LCF, we can express its motion equation in a Schrödinger-like form

$$i\hbar \frac{d}{ds} |\psi_v(s)\rangle = \hat{H}(s) |\psi_v(s)\rangle, \quad (5)$$

where  $|\psi_v(s)\rangle = [v_n(s), v_b(s), v_t(s)]^T$  and the effective Hamiltonian is given by

$$\hat{H}(s) = \hbar \mathbf{B}(s) \cdot \hat{\mathbf{S}}, \quad (6)$$

with an effective magnetic field  $\mathbf{B}(s) = -\kappa(s) \mathbf{b}(s) + \tau(s) \mathbf{t}(s)$  and the generators of the SO(3) rotations

$$\hat{S}_n = \begin{bmatrix} 0 & 0 & 0 \\ 0 & 0 & -i \\ 0 & i & 0 \end{bmatrix}, \quad \hat{S}_b = \begin{bmatrix} 0 & 0 & i \\ 0 & 0 & 0 \\ -i & 0 & 0 \end{bmatrix}, \quad \hat{S}_t = \begin{bmatrix} 0 & -i & 0 \\ i & 0 & 0 \\ 0 & 0 & 0 \end{bmatrix}. \quad (7)$$

Here, the wave vector  $|\psi_v(s)\rangle$  is not necessarily normalized. Its length does not change since the matrix  $\hat{H}(s)$  is Hermitian.

\* lipingyang87@gmail.com

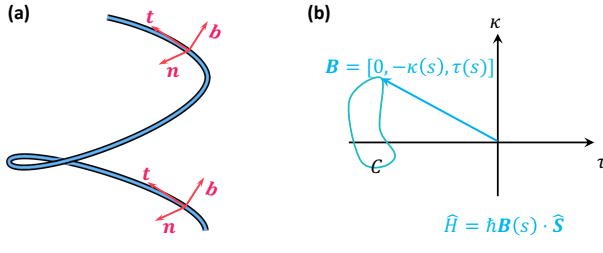


FIG. 1. (a) Parallel transport of the local coordinate frame (LCF) on a curve. (b) Movement of the LCF in the parameter space described by the effective magnetic field  $\mathbf{B}(s) = [0, -\kappa(s), \tau(s)]$  and Hamiltonian  $\hat{H} = \hbar \mathbf{B}(s) \cdot \hat{\mathbf{I}}$ . Here,  $\kappa(s)$  and  $\tau(s)$  are the local curvature and torsion of the curve at  $s$ , and  $\hat{\mathbf{I}}$  is an operator vector composed of generators of the  $\text{SO}(3)$  rotations as given in Eq. (7).

The instantaneous eigen states of  $\hat{H}(s)$  are given by

$$|0\rangle = [0, -\sin \theta(s), \cos \theta(s)]^T, \quad (8)$$

$$|+1\rangle = \frac{1}{\sqrt{2}} [-i, \cos \theta(s), \sin \theta(s)]^T, \quad (9)$$

$$|-1\rangle = \frac{1}{\sqrt{2}} [i, \cos \theta(s), \sin \theta(s)]^T, \quad (10)$$

with corresponding eigenvalues 0 and  $\pm \omega(s)$ . We note that the curvature  $\kappa(s)$ , torsion  $\tau(s)$ ,  $\omega(s) = \sqrt{\kappa^2(s) + \tau^2(s)}$ , and the pitch angle  $\theta(s)$  are all dependent on  $s$  in this case.

Now, we verify that the vector  $\mathbf{v}$  always returns to its initial value after an adiabatic circulation. Round a close curve  $C$  in the  $\mathbf{B}$ -parameter space [see Fig. 1 (b)], the eigenstate  $|n\rangle$  ( $n = 0, \pm 1$ ) of  $\hat{H}$  will accumulate both the dynamical phase  $\alpha_n(C)$  and the Berry's phase  $\gamma_n(C)$ . The Berry's phases for all three states are zero because the corresponding solid angle  $\Omega_n(C)$  in the parameter space vanishes as shown in Fig. 1 (b). The dynamics phase for the three states are given by

$$\alpha_n(C) = -n \oint_C \omega(s) ds = -n \oint_C d\varphi = -2n\pi, \quad n = 0, \pm 1, \quad (11)$$

where we have used the geometric relation  $\omega ds = d\varphi$  for each small segment. By expanding  $|\psi_n\rangle$  with  $\{|n\rangle\}$ , we can verify that  $|\psi_n(\varphi = 2\pi)\rangle = |\psi_n(\varphi = 0)\rangle$ . Thus, in the laboratory reference frame,  $\mathbf{v}$  returns to its initial value round  $C$ , i.e.,  $\mathbf{v}(\varphi = 2\pi) = \mathbf{v}(\varphi = 0)$ . This proves our claim that the LCF remains the same after an adiabatic circulation.

In principle, we can construct a complicated winding path, such that the Berry's for the LCF is not zero as shown in Fig 2. Special care needs to be taken at points  $B$  and  $D$ , at which the curvature  $\kappa(s)$  vanishes and the normal vector  $\mathbf{n}$  is not defined. More details about the non-vanishing Berry's phase are out of our interest in this work. Next, we focus on the rotation of the PCF with respect to the LCF.

*Rotation of the photon coordinate frame*—The wave vector  $\mathbf{k}$  and two transverse polarization unit vectors ( $\mathbf{e}_1$  and  $\mathbf{e}_2$ ) form another coordinate frame—the PCF, which co-moves with the photon. We emphasize that the PCF is not synchronized with the LCF usually. This de-synchronization leads to the rotation of the linear polarization vector of the photon and the geometric phase for circularly polarized light.

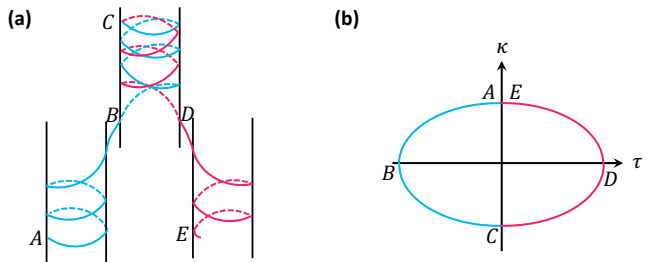


FIG. 2. (a) A winding method of a fiber to obtain non-vanishing Berry's phase for the local coordinate frame (LCF). (b) The path of the LCF in the parameter space. At points  $B$  and  $D$ , the curvature  $\kappa(s)$  of the curve changes sign. At point  $C$ , the sign of the torsion  $\tau(s)$  of the curve flips.

Two successive reflections of the photon in the fiber give an adiabatic transformation of the PCF as shown in Fig. 3 (a). Now we sit on the LCF to study the dynamics of an arbitrary vector  $\mathbf{v}$  co-moving with the PCF. The reflection of the PCF at  $s$  is described by the matrix

$$\hat{P}_t = \begin{bmatrix} -1 & 0 & 0 \\ 0 & -1 & 0 \\ 0 & 0 & 1 \end{bmatrix}, \quad (12)$$

which is the space reversion in the normal plane (i.e.,  $\mathbf{n}\mathbf{b}$ -plane). Here, we have used the fact that the no rotation of the PCF around the  $\mathbf{k}$ -axis occurs under a reflection as shown in Fig. 3 (b). From  $s$  to  $s + ds/2$ , the vector  $\mathbf{v}$  itself remains unchanged. However, the LCF has been rotated by  $\hat{R}(\Delta\varphi/2, \mathbf{e}(s))$ . Thus, from the perspective of the LCF,  $\mathbf{v}$  has been rotated by  $\hat{R}(-\Delta\varphi/2, \mathbf{e}(s))$ . Here, we see the adiabatic evolution of the PCF is described by

$$\hat{U}(\Delta\varphi) = \hat{R}\left(-\frac{\Delta\varphi}{2}, \mathbf{e}(s)\right) \hat{P}_t \hat{R}\left(-\frac{\Delta\varphi}{2}, \mathbf{e}(s)\right) \hat{P}_t. \quad (13)$$

If a fiber is wound in a co-planar path (i.e.,  $\tau(s) = 0$ ), the photon polarization vector propagates by parallel transport as the same as the LCF. This was taken as an axiom by Ross and supported by his experiment [1]. Haldane pointed out this claim follows geometrically by approximating a general fiber path as a sequence of curved co-planar segments joined by straight segments [10]. We now verify this result directly by setting  $\theta = \pi/2$  in Eq. (13). We find that the adiabatic evolution operator always equals the identity matrix, i.e.,  $\hat{U}(\Delta\varphi) = \hat{I}$ . Thus, in the absence of torsion, the PCF maintains synchronization with the LCF.

Now we show that in presence of torsion, the vector  $\mathbf{v}$  co-moving with the PCF rotates around the  $\mathbf{t}$ -axis during propagation. The motion equation of  $\mathbf{v}(\varphi)$  in the LCF is given by

$$\frac{d}{d\varphi} \mathbf{v}(\varphi) = \hat{\mathcal{H}}(\varphi) \mathbf{v}, \quad (14)$$

where

$$\hat{\mathcal{H}}(\varphi) = \lim_{\Delta\varphi \rightarrow 0} \frac{\hat{U}(\Delta\varphi) - \hat{I}}{\Delta\varphi} = \begin{bmatrix} 0 & \cos \theta(\varphi) & 0 \\ -\cos \theta(\varphi) & 0 & 0 \\ 0 & 0 & 0 \end{bmatrix}. \quad (15)$$

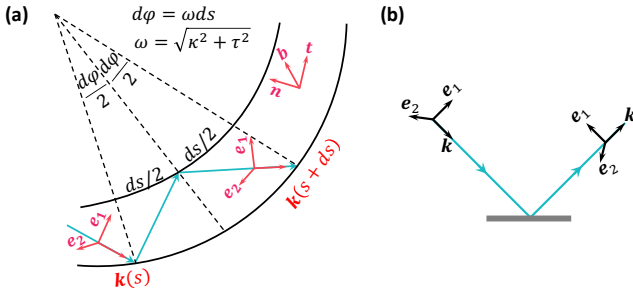


FIG. 3. (a) Two successive reflections in the fiber give an adiabatic transformation of the photon coordinate frame (PCF). (b) The change of the PCF under a reflection.

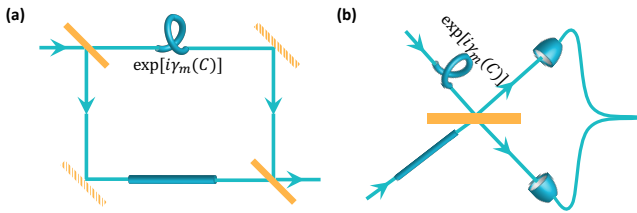


FIG. 4. (a) Detection of the geometric phase  $\gamma_M(C)$  for twisting photons carrying orbital angular momentum via Mach-Zehnder interference. (b) Detection of the geometric phase for twisting photons via Hong-Ou-Mandel interference.

For a single-mode fiber, we assume that the photon enters the fiber nearly parallel to its tangent vector, i.e.,  $\mathbf{k}(0)/|\mathbf{k}| \approx \mathbf{t}(0)$ . The PCF and LCF coincide at the beginning. It follows that the rotation angle of the polarization vector, i.e., the geometric phase for the circularly polarized light after an adiabatic circulation is given by

$$\gamma_{\pm}(C) = \pm \int_0^{2\pi} \cos \theta(\varphi) d\varphi. \quad (16)$$

This explains Tomita and Chiao's experiment [5]. For a uniform helix, the pitch angle  $\theta$  is a constant. Then our phase geometric phase  $\gamma_{\pm}(C) = \pm 2\pi \cos \theta$  recovers Chiao and Wu's results [4]. We emphasize that, in our description,  $\gamma(C)$  is purely geometric and it is not Berry's phase.

*Geometric phase for a twisted photon*—We now apply our method to a twisted photon traveling in a coiled fiber to show that the geometric rotation also occurs on the OAM states. The corresponding geometric phase for a twisted photon carry  $m\hbar$  OAM is given by

$$\gamma_m(C) = m \int_0^{2\pi} \cos \theta(\varphi) d\varphi, \quad (17)$$

which is  $m$  times as large as that of a photon spin state.

A linearly polarized twisted optical pulse or beam propagating in the  $z$ -direction can be generally described by a spectral amplitude function in  $\mathbf{k}$ -space [8, 12]

$$\xi_m(\mathbf{k}) = \eta(k_z, \rho_k) e^{im\varphi_k}, \quad (18)$$

where  $\rho_k = \sqrt{k_x^2 + k_y^2}$ ,  $\varphi_k$  is the azimuthal angle of  $\mathbf{k}$  in the PCF,  $m$  is an integer determining the OAM quantum number, and the function  $\eta$  characterizes the spacial distribution of the photon. For an elegant Laguerre-Gaussian beam, we have [12]

$$\eta(\rho_k, k_z) = \delta(k_z - k) \rho_k^{p+2m} \exp \left\{ -\frac{w_0^2}{4} (1 + i\zeta) \rho_k^2 \right\}, \quad (19)$$

with the center wave vector  $k = |\mathbf{k}|$ , beam waist  $w_0$ , an integer  $p$ , the reduced  $z$ -coordinate  $\zeta = z/z_R$ , and the Rayleigh length  $z_R = k_z w_0^2/2$ . For a diffraction-free Bessel beam, we have  $\eta = \delta(k_z - k \cos \theta_0) \delta(\rho_k - k \sin \theta_0)$  with polar angle  $\theta_0$  [12].

After an adiabatic circulation, we have the transformation relation  $(k_x + ik_y)^m \rightarrow (k_x + ik_y)^m \exp[i\gamma_m(C)]$  if the beam is injected into the fiber along  $\mathbf{t}$ -axis, i.e.,  $\mathbf{e}_z \approx \mathbf{t}(0)$ . By re-expressing the phase factor  $\exp(im\varphi_k) = [(k_x + ik_y)/\rho_k]^m$ , we obtain the geometric phase in Eq. (17) for  $\xi_m(\mathbf{k})$ . After a Fourier transformation, this phase factor  $\exp[i\gamma_m(C)]$  transfers to the corresponding wave-packet function in the real-space [13]. The geometric phase of a standard Laguerre-Gaussian beam [12] can be obtained similarly via the transformation relation for the differential operator  $(\partial_{k_x} + i\partial_{k_y})^m \rightarrow (\partial_{k_x} + i\partial_{k_y})^m \exp[i\gamma_m(C)]$ .

Our predicted geometric phase in Eq. (17) can be observed in the following three interference experiments. (i) Mach-Zehnder interference with an OAM beam as shown in Fig. 4 (a). There are a straight fiber and a coiled fiber with equal length in the two interference channels. Our geometric phase  $\gamma_m(C)$  will lead to the rotation of the interference pattern [14, 15]; (ii) Mach-Zehnder interference with an entangled OAM states  $|\text{MOOM}\rangle = (|1_m, 0\rangle + |0, 1_m\rangle)/\sqrt{2}$  as the input state [16]. Here,  $|1_m\rangle$  denotes the state of a single-photon pulse carrying  $m\hbar$  OAM. The phase  $\gamma_m(C)$  can be measured via the intensity difference of the two output ports; (iii) Hong-Ou-Mandel interference with twisted photon pairs as shown in Fig. 4 (b). The phase  $\gamma_m(C)$  can be measured via the rotation of the  $g^2$ -function [13].

Finally, we note that our predicted geometric phase  $\gamma_m(C)$  can be utilized to construct a Z-gate for OAM-state based quantum computation [17], which has been previously realized via a pair of Dove prisms [18–20]. Previously, entangled twisted photons has been exploited for the super-sensitive measurement of angular displacements [16]. The geometric phase for twisted photons can be used to detect the pitch-angle-related quantities with higher sensitivity via a similar interference strategy.

*Acknowledgments.* The author thanks Professor C. P. Sun for bringing my attention to this issue. This work is funded by National Key R&D Program of China (Grant No. 2021YFE0193500).

---

[1] J. Ross, The rotation of the polarization in low birefringence monomode optical fibres due to geometric effects, *Optical and Quantum electronics* **16**, 455 (1984).

[2] M. Varnham, D. Payne, and R. Birch, Helical-core circularly-birefringent fibres, in *5th European Conference on Optical Communication (ECOC)* (Venice, Italy, 1985) pp. 135–138.

[3] M. V. Berry, Quantal phase factors accompanying adiabatic changes, *Proceedings of the Royal Society of London. A. Mathematical and Physical Sciences* **392**, 45 (1984).

[4] R. Y. Chiao and Y.-S. Wu, Manifestations of berry's topological phase for the photon, *Phys. Rev. Lett.* **57**, 933 (1986).

[5] A. Tomita and R. Y. Chiao, Observation of berry's topological phase by use of an optical fiber, *Phys. Rev. Lett.* **57**, 937 (1986).

[6] M. V. Berry, Quantum adiabatic anholonomy, in *Anomalies phases, defects*, edited by U. M. Bregola, M. G., and M. G. (Bibliopolis, Naples, 1990) pp. 125–181.

[7] L. Allen, M. W. Beijersbergen, R. J. C. Spreeuw, and J. P. Woerdman, Orbital angular momentum of light and the transformation of laguerre-gaussian laser modes, *Phys. Rev. A* **45**, 8185 (1992).

[8] L.-P. Yang and Z. Jacob, Non-classical photonic spin texture of quantum structured light, *Communications Physics* **4**, 221 (2021).

[9] M. Berry, Interpreting the anholonomy of coiled light, *Nature* **326**, 277 (1987).

[10] F. Haldane, Path dependence of the geometric rotation of polarization in optical fibers, *Optics letters* **11**, 730 (1986).

[11] M. P. Do Carmo, *Differential geometry of curves and surfaces: revised and updated second edition* (Courier Dover Publications, 2016) Chap. 1.

[12] J. Enderlein and F. Pampaloni, Unified operator approach for deriving hermite-gaussian and laguerre-gaussian laser modes, *JOSA A* **21**, 1553 (2004).

[13] L.-P. Yang and D. Xu, Quantum theory of photonic vortices and quantum statistics of twisted photons, *Phys. Rev. A* **105**, 023723 (2022).

[14] J. Guo, B. Guo, R. Fan, W. Zhang, Y. Wang, L. Zhang, and P. Zhang, Measuring topological charges of Laguerre–Gaussian vortex beams using two improved Mach–Zehnder interferometers, *Optical Engineering* **55**, 1 (2016).

[15] P. Kumar and N. K. Nishchal, Modified mach-zehnder interferometer for determining the high-order topological charge of laguerre-gaussian vortex beams, *J. Opt. Soc. Am. A* **36**, 1447 (2019).

[16] A. K. Jha, G. S. Agarwal, and R. W. Boyd, Supersensitive measurement of angular displacements using entangled photons, *Phys. Rev. A* **83**, 053829 (2011).

[17] A. Babazadeh, M. Erhard, F. Wang, M. Malik, R. Nouroozi, M. Krenn, and A. Zeilinger, High-dimensional single-photon quantum gates: Concepts and experiments, *Phys. Rev. Lett.* **119**, 180510 (2017).

[18] A. De Oliveira, S. Walborn, and C. Monken, Implementing the deutsch algorithm with polarization and transverse spatial modes, *Journal of Optics B: Quantum and Semiclassical Optics* **7**, 288 (2005).

[19] X. L. Wang, X. D. Cai, Z. E. Su, M. C. Chen, D. Wu, L. Li, N. L. Liu, C. Y. Lu, and J. W. Pan, Quantum teleportation of multiple degrees of freedom of a single photon, *Nature* **518**, 516 (2015).

[20] Y. Zhang, F. S. Roux, T. Konrad, M. Agnew, and A. Forbes, Engineering two-photon high-dimensional states through quantum interference, *Science Advances* **2**, e1501165 (2016).